

# THE CRYSTALLISATION OF CALCIUM PHOSPHATE GLASS CONTAINING VANADIUM OXIDE

VLADIMIR D. ŽIVANOVIC, MIHAJLO B. TOŠIĆ, NIKOLA S. BLAGOJEVIĆ\*,  
SNEŽANA R. GRUJIĆ\*, MIĆO M. MITROVIĆ\*\*

*Institute for the Technology of Nuclear and Other Mineral Raw Materials, 86 Franchet d, Esperey, 110 00 Belgrade, Serbia*

*\*Faculty of Technology and Metallurgy, 4 Karnegijeva, 110 00 Belgrade, Serbia*

*\*\*Faculty of Physics, 12-16 Akademski Trg, 110 00 Belgrade, Serbia*

E-mail: v.zivanovic@itnms.ac.yu

Submitted July 10, 2006; accepted December 10, 2006

**Keywords:** Phosphate glass, Vanadium oxide, Crystallisation

*The crystallisation behaviour of calcium phosphate glass containing vanadium oxide was studied. Glass with a molar ratio of  $[CaO]/[P_2O_5] = 1.13$  and a  $V_2O_5$  content of 8 mol.% was prepared for the experiments. The crystallisation of bulk glass samples was performed under isothermal conditions at  $T = 650\text{--}820^\circ C$ . The surface crystallisation mechanism of studied glass with dendritic growth of the primary  $\alpha\text{-}Ca_2P_2O_7$  phase was observed. In all crystallised samples,  $\beta\text{-}Ca_2P_2O_7$  and  $VP_2O_7$  appeared as the secondary phases. In the investigated temperature range, crystal growth rates  $9 \times 10^{-9} \text{--} 2.14 \times 10^{-6}$  m/s were determined. The temperature dependence of the crystal growth rate makes possible to calculate activation energy  $E_a = 407 \pm 30$  kJ/mol of crystallization. The experimental data were compared with those estimated by using a theoretical model of the crystal growth rate and good agreement between the results was found.*

## INTRODUCTION

Among different materials for medical use as implants in dental, orthopaedic and bone surgery, glasses and especially glass-ceramics based on the  $CaO\text{-}P_2O_5$  system have become very important, because of their bioactivity and biocompatibility [1,2].

It has been reported earlier that calcium phosphate glass-ceramics can be obtained conventionally by controlled crystallisation of the parent glass or by the simultaneous sintering and crystallisation of fine glass powders [3]. However, most phosphate glasses do not fulfil the criterion required for controlled crystallisation due to their specific structure. Metaphosphate glasses the structure of which consists of metaphosphate chains or rings formed by  $Q^2$  groups, do not tend to phase separate [4,5].

The structure of phosphate glasses can be modified by introducing other metallic oxides that lead to changes in crystallisation behaviour. By increasing the content of modifying oxides, polyphosphate glasses (invert phosphate glasses) with  $P_2O_5 < 50$  mol.%, can be obtained. These glasses tend to crystallise much more rapidly due to their structure - very small molecular structural groups (orthophosphate groups) [6].

James *et al.* [7] have investigated the crystallisation behaviour of the binary  $CaO\text{-}P_2O_5$  system, and only the surface crystallisation mechanism was observed. Watanabe *et al.* [8] have shown that the addition of  $Al_2O_3$  to glass with a molar ratio of  $(CaO)/(P_2O_5) < 1$  enables its

volume crystallisation. Tasic *et al.* have detected that the addition of  $TiO_2$  and  $Al_2O_3$  to glass with the molar ratio  $(CaO)/(P_2O_5) = 0.88$  caused a change in the crystallisation mechanism from a surface to a volume one [9]. Hosono *et al.* [10] registered volume crystallisation by using  $TiO_2$  as an additive in glass with a molar ratio  $(CaO)/(P_2O_5) > 1$ . To promote the volume crystallisation of the glasses with  $(CaO)/(P_2O_5) \geq 1$ , Nan *et al.* [5] and Reaney *et al.* [11] used  $TiO_2$  and  $Al_2O_3$  as effective nucleating agents.

Depending on the  $(CaO)/(P_2O_5)$  ratio, different crystalline phosphate phases can be precipitated in the glass matrix during crystallisation. Mostly, one of the polymorphic forms of the  $Ca_2P_2O_7$  phase ( $\alpha$ ,  $\beta$ ,  $\gamma$ ) could be observed as the primary phase that crystallised [12]. The content and properties of each phase strongly define the properties of the multiphase system obtained. Glass ceramics containing calcium pyrophosphate ( $\beta$ - $Ca_2P_2O_7$ ) are reported to be biocompatible [13].

Tasic *et al.* registered the presence of  $\alpha$ - $Ca_2P_2O_7$  as the primary phase and of  $\beta$ - $Ca_2P_2O_7$  and  $VP_2O_7$  as secondary ones in surface-crystallised calcium phosphate glasses containing 5 to 13 mol.% vanadium oxide [14]. As reported, the content of  $V_2O_5$  strongly determined the content of  $\beta$ - $Ca_2P_2O_7$  in the crystallised glass. The aim of the current investigation was to study in detail the crystallisation behaviour of an invert calcium phosphate glass of the composition  $49CaO\cdot43P_2O_5\cdot8V_2O_5$  (mol.%). The experiments were performed on bulk glass samples under isothermal conditions.

## EXPERIMENTAL

Reagent grade CaO, V<sub>2</sub>O<sub>5</sub> and an aqueous solution of orthophosphoric acid (85 wt.% H<sub>3</sub>PO<sub>4</sub>) were used to prepare the mixture for glass melting. The preparation procedure involved: a) mixing and homogenisation of the solid components, b) the addition of distilled water and a solution of H<sub>3</sub>PO<sub>4</sub> with constant mixing of the mixture, c) drying of the suspension obtained in an electric furnace at 200°C, d) pulverisation of the dried precipitate.

Glass melting was performed at  $T = 1200^\circ\text{C}$  for  $t = 60$  min in an electric furnace using a Pt-crucible. The melt was cast on a steel plate and cooled in air. The molten sample solidified as homogenous black glass. The powder samples for the experiments were prepared by crushing and milling the compact glass in an agate mortar and then sieving it to an appropriate grain size. Bulk samples of the dimension of 1×1×1 cm, were prepared by cutting a glass block with a diamond saw.

The chemical composition of the glass was determined by AAS and UV/VIS spectrometry. AAS PERKIN ELMER 703 and PHILIPS UV/VIS 8610 spectrophotometer were used.

The crystallisation behavior of the glass under non-isothermal conditions was analysed using a DTA-Netzsch STA 409 EP device with Al<sub>2</sub>O<sub>3</sub> powder as the reference material. Glass powder samples of 0.50–0.63 mm (100 mg) were heated at a rate of  $v = 2\text{--}20^\circ\text{C}/\text{min}$  up to 1100°C.

The glass transition temperature ( $T_g$ ) and dilatometric softening temperature ( $T_{om}$ ) were determined using a Bähr Geratebau GmbH, Tip 8025 dilatometer in accordance with ISO 7884-8 [15].

Isothermal crystallisation experiments on compact glass samples were performed in an electric furnace with automatic regulation and a temperature accuracy of  $\pm 2^\circ\text{C}$ . The samples were heated at crystallisation temperatures in the range  $T_c = 650\text{--}820^\circ\text{C}$  for different times  $t_c = 20\text{--}6000$  min and then subjected to X-ray powder diffraction (XRD) and scanning electron microscopy (SEM).

The phase composition of the crystallised samples was analysed by the XRD method using a Philips PW-1710 automated diffractometer with a Cu K $\alpha$  radiation tube operating at 40 kV and 32 mA. Data were collected from 5 to 70° 2 $\theta$ , with step size of 0.02° and a counting time of 1 s per step. The quantitative amounts of the crystalline phases in the glass sample were determined using the full structure matching mode of the Rietveld refinement technique [16], using the FULLPROF programme [17].

Selected compact samples were chosen for investigation of the microstructure by SEM analyses (Jeol JSM 840 A). The samples were gold sputtered in Jeol JFC 1100 ion sputter. Micrographs of the exterior and interior (fracture) surfaces of the crystallised samples were recorded.

## RESULTS AND DISCUSSION

## Chemical composition of the glass

Table 1 shows the initial composition of the glass and its chemical analysis.

It may be seen from Table 1 that a glass with the ratio (CaO)/(P<sub>2</sub>O<sub>5</sub>) = 1.13 was obtained. The low content of V<sub>2</sub>O<sub>5</sub> (8.05 mol.%) enables this glass to be considered as a binary glass. The vanadium ion can exist in different valence states in glasses, so it may be attributed the role of modifier or network former [18]. Regarding its low content in this glass, the role of modifier chosen for this ion as well as for the Ca<sup>2+</sup> ion. In this case the glass was treated as a binary glass 0.57MeO·0.43P<sub>2</sub>O<sub>5</sub> [(MeO) = (CaO) + (V<sub>2</sub>O<sub>5</sub>)] having the ratio (O)/(P) = 3.165. Consequently, this glass belongs to polyphosphate glasses, the structure of which consists of phosphate chains containing Q<sup>2</sup> tetrahedra (two bridging oxygen atoms) and terminated Q<sup>1</sup> tetrahedra (one bridging oxygen atom). For binary glasses  $x\text{MeO}\cdot(1 - x)\text{P}_2\text{O}_5$  with the molar fraction  $x$  of 0.5 <  $x$  < 0.67, the fraction of Q<sup>1</sup> and Q<sup>2</sup> tetrahedra are given as  $f(\text{Q}^1) = (2x - 1)/(1 - x)$  and  $f(\text{Q}^2) = (2 - 3x)/(1 - x)$  and the average tetrahedron chain length ( $L_{av}$ ) is given as  $L_{av} = 2(1 - x)/(2x - 1)$  [6]. Accordingly,  $f(\text{Q}^1) = 0.326$ ,  $f(\text{Q}^2) = 0.674$  and  $L_{av} = 6.14$  were calculated for this glass.

Regarding the values obtained, it may be concluded that the structure of this glass consists of phosphate chains containing six tetrahedra, where four of them contain two bridging oxygens, and two terminal tetrahedra with one bridging oxygen. The modifier ions are placed in the cavities between tangled phosphate chains.

Table 1. Composition of the glass.

oxides	CaO (mol %)	P <sub>2</sub> O <sub>5</sub> (mol %)	V <sub>2</sub> O <sub>5</sub>	(CaO)/(P <sub>2</sub> O <sub>5</sub> )
initial	49	43	8	1.14
analysed	48.86	43.09	8.05	1.13

## Non-isothermal crystallisation

The DTA curves were recorded at different heating rates of 2–20°C/min. Three notable features of such DTA curves are: (i) an endothermic shoulder corresponding to the glass transition temperature,  $T_g$ , (ii) one exo peak in the temperature range of 670–723°C representing the crystallization of glass and (iii) one broad endothermic peak in the range of 870–928°C, indicating the melting of crystals, as the liquidus temperature  $T_l$  is approached. The DTA curves recorded at heating rates of  $v = 5$  and 10°C/min are presented in Figure 1. The significant peak temperatures are summarized in Table 2.

The dilatometric curve is presented in Figure 2. A glass transition temperature of  $T_g = 540^\circ\text{C}$  and dilatometric softening temperature of  $T_{om} = 572^\circ\text{C}$  were determined.

### Isothermal crystallisation of the bulk glass

Bulk glass samples, isothermally heated in the temperature range of  $T = 650\text{--}820^\circ\text{C}$  for different times  $t_c = 20\text{--}6000$  min, were subjected to XRD analysis. The diffraction pattern of the glass sample heated at  $T = 650^\circ\text{C}$  for  $t_c = 100$  h was shown that three crystalline phases were formed in the glass matrix during crystallisation:  $\alpha\text{-Ca}_2\text{P}_2\text{O}_7$  [19],  $\beta\text{-Ca}_2\text{P}_2\text{O}_7$  (JCPDS 33-0297) and  $\text{VP}_2\text{O}_7$  (JCPDS 44-0066).  $\alpha\text{-Ca}_2\text{P}_2\text{O}_7$  was formed as the primary phase, followed by  $\beta\text{-Ca}_2\text{P}_2\text{O}_7$  and  $\text{VP}_2\text{O}_7$  as secondary ones. A Rietveld profile matching mode fitting plot of this sample is presented in Figure 3, while the results of the fitting are shown in Table 3. These phases appeared in all the glass samples isothermally treated at different temperatures and times.

### SEM analysis

The evolution of microstructure of selected bulk glass samples, crystallised under the conditions presented above, was investigated by scanning the glass surfaces. Some characteristic micrographs are shown in Figures 4, 5 and 6.

Table 2. The significant temperatures determined by DTA.

Run	$T_g$ ( $^\circ\text{C}$ )	$T_p$ ( $^\circ\text{C}$ )	$T_i$ ( $^\circ\text{C}$ )
DTA, $v = 5^\circ\text{C}/\text{min}$	539	683	890
DTA, $v = 10^\circ\text{C}/\text{min}$	540	690	892

Table 3. The most important crystallographic parameters for crystalline phases, obtained from Rietveld refinement of XRD pattern.

Phase	Unit cell parameters			Reliability factors			Quantitative volume fraction (%)
	a (Å)	b (Å)	c (Å)	$\beta$ ( $^\circ$ )	RB(%)	RF(%)	
$\alpha\text{-Ca}_2\text{P}_2\text{O}_7$	12.637(2)	8.527(1)	5.3105(8)	90.17(1)	12.1	6.30	52.59
$\beta\text{-Ca}_2\text{P}_2\text{O}_7$	6.688(2)	6.688(2)	24.146(4)	90	12.8	8.52	27.23
$\text{VP}_2\text{O}_7$	10.982(2)	10.982(2)	4.2790(7)	90	11.4	8.17	20.18

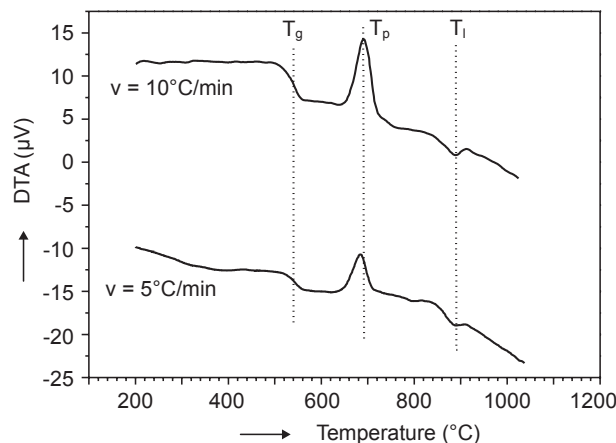


Figure 1. DTA curves recorded at 5 and 10°C/min for a sample particle size of 0.5-0.63 mm.

The SEM micrograph (Figure 4) of the interior (fracture) surface of a fully crystallised glass sample at  $T = 650^\circ\text{C}$  for  $t = 60$  h shows a needle-like crystal structure. The surface crystallisation mechanism of the glass studied is clearly seen in the micrograph, Figure 5. As may be seen, the crystallised layer is formed by crystal growth on the faceted crystal-melt boundaries inward from the external surface of the glass sample annealed at  $T = 650^\circ\text{C}$  for  $t = 5$  h. A typical directional crystal growth (dendritic morphology) is obvious in Figure 6.

### Crystal growth kinetics

The SEM data were used to calculate the crystal growth rate. Accordingly, the crystal layer thickness was measured for each temperature and time of crystallisation.

The time dependence of the crystal layer thickness at selected temperatures  $T = 650$  and  $700^\circ\text{C}$  is shown in Figure 7. A linear relation between the crystal layer thickness and the growth time was obtained. The slopes of the lines define the growth rate of the crystallised layer at denoted temperatures. The temperature dependence of the growth rate of the crystallised layer is presented in Figure 8, which revealed that up to  $T_c = 750^\circ\text{C}$ , the growth rate of the crystal layer was slightly changed. An abrupt change of the growth rate was noticeable in the temperature range  $T_c = 750\text{--}820^\circ\text{C}$ .

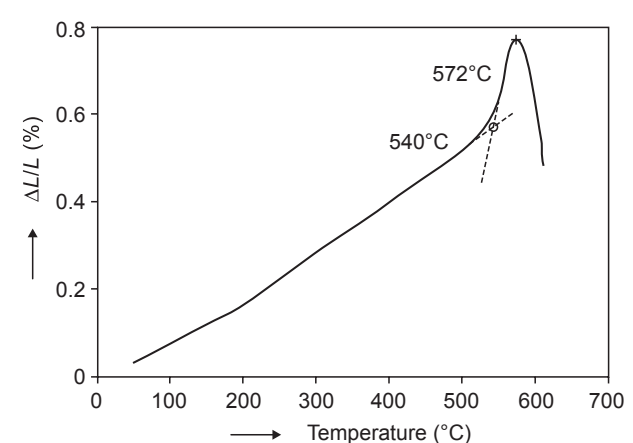


Figure 2. Dilatometric curve of the glass.

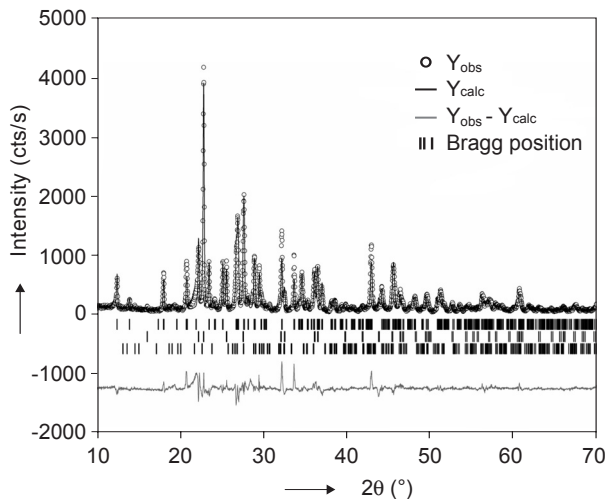


Figure 3. Rietveld refinement plot of a glass sample annealed at  $T = 650^\circ\text{C}$  for  $t = 100$  h.

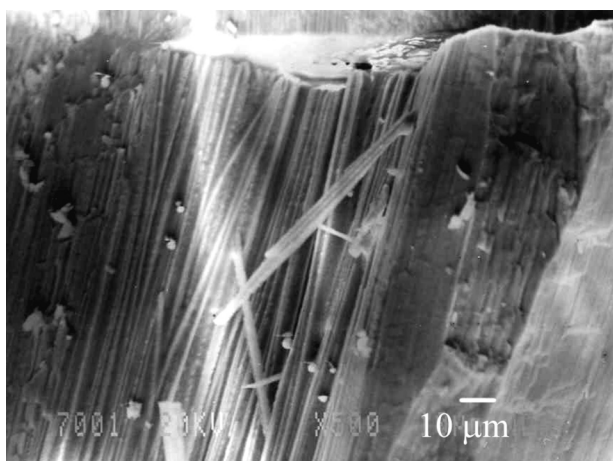


Figure 4. SEM micrograph of a glass sample annealed at  $T = 650^\circ\text{C}$  for  $t = 60$  h.

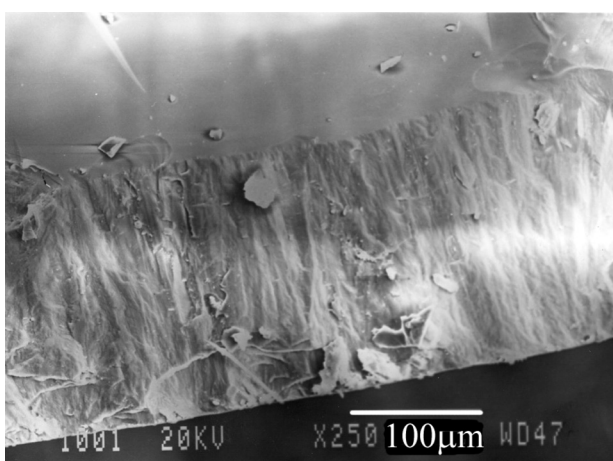


Figure 5. SEM micrograph of a glass sample annealed at  $T = 650^\circ\text{C}$  for  $t = 5$  h.

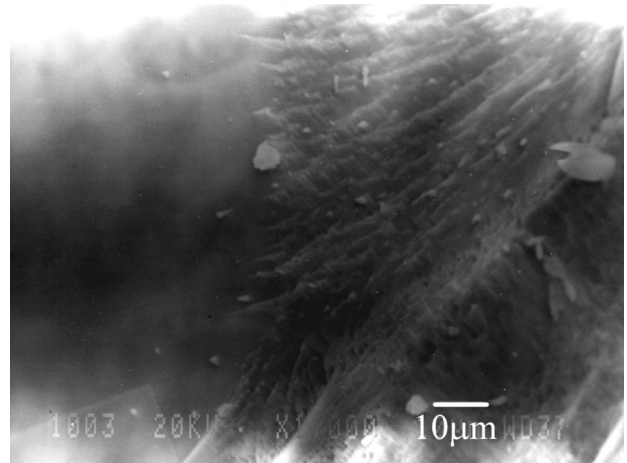


Figure 6. SEM micrograph of a glass sample annealed at  $T = 650^\circ\text{C}$  for  $t = 10$  h.

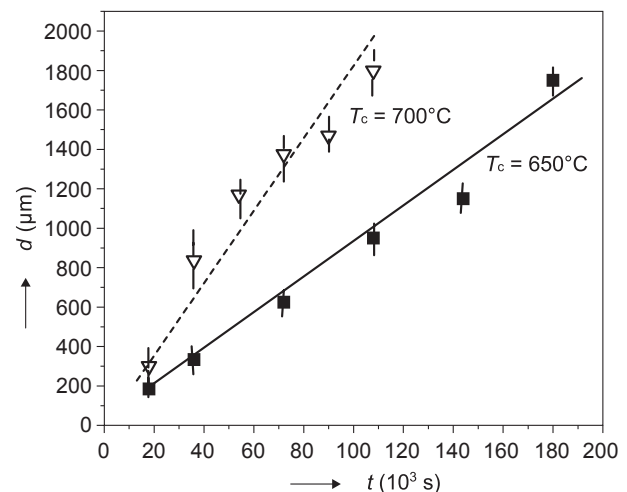


Figure 7. Crystal layer thickness vs. growth time at selected temperatures.

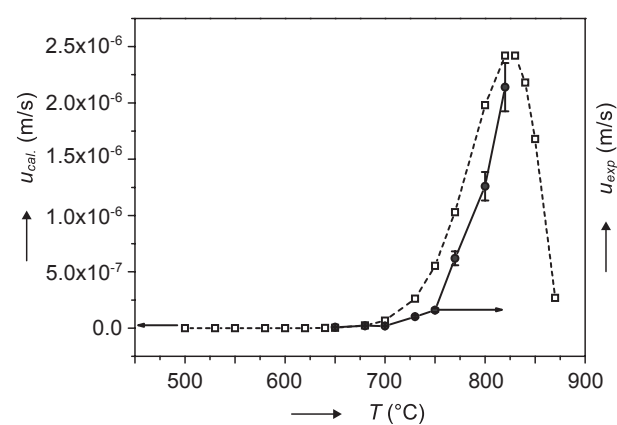


Figure 8. The experimental ( $u_{\text{exp}}$ ) and calculated ( $u_{\text{cal.}}$ ) curves of the crystal growth rate.

As reported earlier, the molar entropy of fusion of  $\text{Ca}_2\text{P}_2\text{O}_7$  crystals is  $\Delta S_m = 62.015 \text{ J/mol K}$  [20]. Using the Jackson criterion,  $\Delta S_m > 4R$ , the most closely packed interface planes should be smooth on an atomic scale, so that the screw dislocation growth mechanism of  $\alpha\text{-Ca}_2\text{P}_2\text{O}_7$  can be considered. Accordingly, the crystal growth rate can be presented using an equation of the form [21]:

$$u = K (\Delta T)^{2(1-\varepsilon)} \exp(-E_a/RT) \quad (2)$$

where  $u$  is the crystal growth rate;  $0 < \varepsilon < 1$  and the parameters  $\varepsilon$ ,  $K$  and  $E_a$  are independent of  $T$ , and  $\Delta T = T_l - T$ , where  $T_l$  is the liquidus temperature.

The growth rate data (Figure 8), and the liquidus temperature ( $T_l$ ), previously estimated from the DTA curve, can be fitted by the least-squares method to Equation (2) in the form:

$$\ln[u/(\Delta T)^{2(1-\varepsilon)}] = \ln K - E_a/RT \quad (3)$$

The activation energy of crystal growth  $E_a$  was calculated from the slope of the line obtained by plotting  $\ln[u/(\Delta T)^2]$  vs.  $1/T$  ( $\varepsilon = 0$ ).

To compare the experimental results with theoretical considerations, the curve of the crystal growth rate was calculated by using an equation of the form [22]:

$$u = fv\gamma[1 - \exp(-\Delta G/RT)] \quad (4)$$

where  $f$  is the fraction of preferred growth sites;  $v$  - the frequency factor for transport at the crystal-liquid interface;  $\gamma$  - the distance advanced by the interface (usually taken as the molecular diameter);  $\Delta G$  - the thermodynamic force for crystallisation, i.e. the difference between the free energies of the undercooled melt and the crystalline phase per mol,  $T$  - the absolute temperature,  $R$  - the universal molar gas constant.

Parameter  $f$  was calculated using the equation:

$$f = \Delta T/2\pi T_m = (1 - T_r)/2\pi \quad (5)$$

where  $\Delta T = T_m - T$  (undercooling);  $T_r \equiv T/T_m$ ;  $T_m$  - melting temperature

The value of  $v$  may be expressed as:

$$v = v_0 \exp(-\Delta G_D/RT) \quad (6)$$

where  $v_0$  is the vibrational frequency of the growth controlling atoms;  $\Delta G_D$  - the activation free energy for diffusion across the interface.

Taking that the molecular mobility necessary for crystal growth is similar to the transport of molecules in the bulk melt, the Stokes - Einstein relation between the effective coefficient of diffusion and the viscosity can be used. Accordingly,  $\Delta G_D \approx \Delta G_\eta = \Delta H_\eta - T \Delta S_\eta$ , where  $\Delta G_\eta$  is the activation free energy for viscous flow. This relation enables the estimation of  $v$  by using the viscosity data. The viscosity of glass melts can be well described by the empirical Vogel-Fulcher-Tamann equation (VFT):

$$\log \eta = A + B / (T - T_0) \quad (7)$$

where  $A$ ,  $B$  and  $T_0$  are empirical parameters. This equation corresponds to the temperature dependence of the activation energy of viscous flow in the form:

$$\eta = \eta_0 \exp(\Delta G_\eta/RT) \quad (8)$$

where:

$$\eta_0 = kT/l^3 v_0 \quad (9)$$

When taking Equations (7-9), Equation (6) can be expressed as:

$$v = kT/l^3 10^4 \cdot \exp[-2.3B/(T - T_0)] \quad (10)$$

where  $k$  is the Boltzman constant;  $l$  - the P-O bond length.

Neglecting the difference of the specific heats of the crystalline and liquid phases, by using the Turnbull linear approximation for  $\Delta G$  [23],  $\Delta G/RT$  can be written as:

$$\Delta G/RT = \Delta S_r (1/T_r - 1); \Delta S_r = \Delta S_m/R \quad (11)$$

The replacement of Equations (10) and (11) into Equation (4) yields the following equation for the crystal growth rate:

$$u = \left( \frac{1 - T_r}{2\pi} \right) \left( \frac{kT}{l^3 10^4} \right) \lambda \cdot \exp\left( \frac{-2.3B}{T - T_0} \right) \left\{ 1 - \exp\left[ -\Delta S_r \left( \frac{1}{T_r} - 1 \right) \right] \right\} \quad (12)$$

Equation (12) was used to calculate the crystal growth rate  $u$  in the temperature range  $T = 620-900^\circ\text{C}$ . The parameters utilized for the calculation are presented in Table 4.

Table 4. Data used for the numerical calculation of crystal growth rate  $u$ .

$k = 1.38059 \times 10^{-23} \text{ J/K}$	$A^{**} = -4.7969$
$l^* = 1.58 \times 10^{-10} \text{ m}$	$B^{**} = 4321.7$
$\lambda = 5 \times 10^{-10} \text{ m}$	$T_0^{**} = 558.9$
$T_l = 1163.16 \text{ K}$	$\Delta S_m = 62.015 \text{ J/mol K}$

\* bond length bridging P - O [24]

\*\*  $\log \eta = A + B / (T - T_0)$  fitted using temperatures  $T_g$ ,  $T_{om}$  and  $T_l$  experimentally determined by DTA and dilatometry.

The calculated curve of the crystal growth rate is also presented in Figure 8. As can be seen in this figure, the curves match at  $T < 700^\circ\text{C}$ . For  $T > 700^\circ\text{C}$ , a difference appeared between the experimental and calculated curves. Such a discrepancy could be explained by experimental error in the crystal growth rate determination. Moreover, the crystallisation experiments were carried out at temperatures above  $T_{om}$  (the dilatometric softening temperature), so that at  $T > 700^\circ\text{C}$  the glass sample dimensions changed markedly, which influenced the measurement of the crystal layer thickness.

Based on all the growth rate data obtained, the activation energy for crystal growth  $E_a$  was determined from the plot in Figure 9. The obtained values of  $E_a$  are presented in Table 5.

Table 5. Activation energy of crystal growth.

Crystal growth rate	$E_a$ (kJ/mol)
$u_{exp}$	$407 \pm 30$
$u_{cal.}$	$454 \pm 10$

The obtained values for  $E_a$  are in agreement with the activation energy determined for the crystal growth of  $\beta\text{-Ca}_2\text{P}_2\text{O}_7$  in calcium phosphate glass doped with  $\text{Al}_2\text{O}_3$  and  $\text{TiO}_2$  [25]. For this glass values of  $E_a = 452 \pm 17$  kJ/mol and  $E_a = 421 \pm 16$  kJ/mol were determined for isothermal and non - isothermal crystallisation conditions respectively. These results indicate, that the formation of calcium phosphate crystalline phases governs the whole process of crystallisation of calcium phosphate glass doped with  $\text{V}_2\text{O}_5$ .

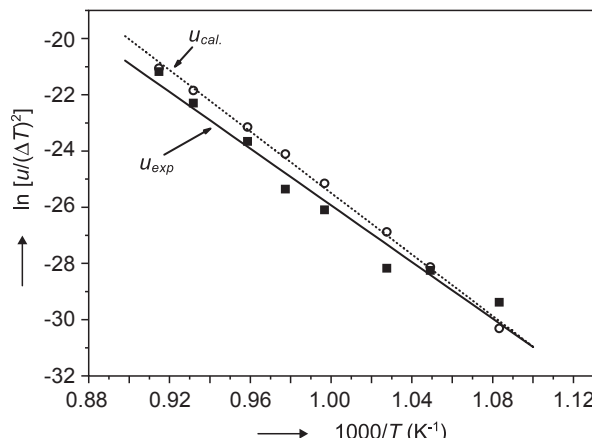


Figure 9. The plot of  $\ln [u/(\Delta T)^2]$  vs.  $1/T$ .

## CONCLUSIONS

The crystallisation behaviour of invert phosphate glass with a molar ratio of  $(\text{CaO})/(\text{P}_2\text{O}_5) = 1.13$  and a  $\text{V}_2\text{O}_5$  content of 8 mol.% was studied. The surface crystallisation mechanism of this glass was determined to be dominant.

Three crystalline phases were formed during crystallisation in the glass matrix, whereby  $\alpha\text{-Ca}_2\text{P}_2\text{O}_7$  was formed as the primary phase, followed by  $\beta\text{-Ca}_2\text{P}_2\text{O}_7$  and  $\text{VP}_2\text{O}_7$  as secondary ones with the volume ratio estimated as 52.59, 27.23 and 20.18 respectively. A den-

dritic morphology of the crystal growth of the primary  $\alpha\text{-Ca}_2\text{P}_2\text{O}_7$  phase on faceted crystal-melt boundaries was observed. Accordingly, the model of the screw dislocation mechanism of the growth of the  $\alpha\text{-Ca}_2\text{P}_2\text{O}_7$  phase was considered. The kinetic parameters of crystal growth obtained from the experimental data are in good agreement with those determined by the theoretical model. Also, there was good agreement between the experimental data of the glass studied and the results previously obtained for the crystallisation of the  $\beta\text{-Ca}_2\text{P}_2\text{O}_7$  phase in the calcium phosphate glass containing  $\text{Al}_2\text{O}_3$  and  $\text{TiO}_2$ .

## References

1. Hench L.L.: Ceramurgia 5, 253 (1977).
2. Zhang Y. Santos J.D.: J. Non-Cryst.Solids 272, 14 (2000).
3. Dias A. G., Tsuru K. , Hayakawa., Lopes M. A., Santos J.D., Osaka A.: Glass Technol. 45, 78 (2004).
4. Vogel W., Holand W., Angw: Chem.Int.Ed.Engl. 26, 527 (1987).
5. Nan Y. , Lee W.E., James P.F.: J.Am.Ceram.Soc. 75, 1641 (1992).
6. Brown R.K.: J.Non.Cryst.Solids 263/264, 1 (2000).
7. James P. F. , Iqbal Y. , Jais U. S., Jordery S., Lee W.E.: J.Non.Cryst.Solids 219, 17 (1977).
8. Watanabe A., Mitsudou M., Kihara S, Abe J.: J.Am. Ceram.Soc. 72, 1499 (1989).
9. Tošić M.B., Dimitrijević R.Ž., Mitrović M.M., Blagojević N.S.: J.Mater.Sci. 37, 4369 (2002).
10. Hosono H., Zang Z, Abe Y.: J.Amer.Ceram.Soc. 75, 1587 (1989).
11. Reaney L.M., James P.F, Lee W.E.: J.Am.Ceram.Soc. 79, 1934 (1996).
12. Webb N.C.: Acta Crystallogr. 21, 942 (1966)
13. Ryu H.S., Youn H.J., Chang B.S., LeeC.K., Chung. S.S.: Biomaterials 23, 909 (2002).
14. Tosić M.B., Živanović V.D., Blagojević N.S.: Phys.Chem. Glasses 45, 160 (2004).
15. International standard ISO 7884-8:1987 (E)
16. Rietveld H.M.; J.Appl.Cryst. 2, 65 (1969).
17. Rodriguez-Carvajal J.: *Users guide to program FULLPROF*, 2004-LLB-JRC (Laboratoire León Brillouin, CEA-CNRS, Centre d'Etudes de Saclay, Gif sur Yvette, France).
18. Vogel W.: *Glaschemie*, 2<sup>nd</sup> ed., VEB , Leipzig, 1983.
19. Calvo C.: Inorganic Chemistry 7, 1345 (1968).
20. Hsc Chemistry.: (Outokumpu Research O4 , Finland, 1993).
21. Hillig W.B., Turnbull D.: J. Chem.Phys. 25, 914 (1956).
22. Kingery W.D., Bowen H.K., Uhlmann D.R.: *Introduction to Ceramics*, Wiley, New York 1976
23. Turnbull D.: J.Appl.Phys. 21, 1022 (1950).
24. Hope U., Walter G., Bartz A., Stachel D., Hannon A.C.: J.Phys.Cond.Matter 10, 261 (1998).
25. Tosić M.B., Dimitrijević R.Ž., Mitrović M.M.: J.Mater. Sci. 38, 1983 (2003).

KRYSTALIZACE SKLA FOSFOREČNANU VÁPENATÉHO  
S OBSAHEM OXIDU VANADIČITÉHO

VLADIMIR D. ŽIVANOVIC, MIHAJLO B. TOŠIĆ,  
NIKOLA S. BLAGOJEVIĆ\*, SNEŽANA R. GRUJIĆ\*,  
MIĆO M. MITROVIĆ\*\*

*Institute for the Technology of Nuclear  
and Other Mineral Raw Materials,  
86 Franchet d, Esperey, 11000 Belgrade, Serbia*  
*\*Faculty of Technology and Metallurgy,  
4 Karnegijeva, 11000 Belgrade, Serbia*  
*\*\*Faculty of Physics,  
12-16 Akademski Trg, 11000, Belgrade, Serbia*

Zkoumalo se krystalizační chování skla fosforečnanu vápenatého obsahujícího oxid vanadičitý. Pro experiment bylo připraveno sklo s molárním poměrem  $(\text{CaO})/(\text{P}_2\text{O}_5) = 1,13$  a obsahem  $\text{V}_2\text{O}_5$  8 mol.%. Krystalizace velkých vzorků skla proběhla za izotermických podmínek při  $T = 650\text{--}820^\circ\text{C}$ . Byl pozorován mechanismus povrchové krystalizace zkoumaného skla se stromečkovým růstem primární fáze  $\alpha\text{-Ca}_2\text{P}_2\text{O}_7$ . Ve všech zkrytalizovaných vzorcích se jako sekundární fáze objevil  $\beta\text{-Ca}_2\text{P}_2\text{O}_7$  a  $\text{VP}_2\text{O}_7$ . Ve zkoumaném teplotním intervalu byl zjištěn růst krystalů o rychlosti  $9 \times 10^{-9}\text{--}2,14 \times 10^{-6}$  m/s. Teplotní závislost na rychlosti růstu krystalů umožňuje vypočítat aktivační energii krystalizace  $E_a = 407 \pm 30$  kJ/mol. Experimentální data byla porovnána s údaji vypočtenými podle teoretického modelu rychlosti krystalového růstu a mezi výsledky byla zjištěna vysoká úroveň shody.

---

Book review

---

MULTIPHYSICS MODELLING WITH FINITE ELEMENT METHODS

*William B. J. Zimmerman*

*World Scientific Publishing,  
New Jersey/London/Singapore 2006  
422 pages, hardcover, price: 41.- GBP  
ISBN 981-256-843-3*

flow, electrokinetic, microfluidic networks, plasma dynamics, and corrosion chemistry.

As a revision of Process Modelling and Simulation with Finite Element Methods, this book uses the very latest features of Comsol Multiphysics. There are new case studies on multiphase flow with phase change, plasma dynamics, electromagnetohydrodynamics, microfluidic mixing, and corrosion. In addition, major improvements to the level set method for multiphase flow to ensure phase conservation is introduced.

Finite element methods for approximating partial differential equations that arise in science and engineering analysis find widespread application. Numerical analysis tools make the solutions of coupled physics, mechanics, chemistry, and even biology accessible to the novice modeler. Nevertheless, modelers must be aware of the limitations and difficulties in developing numerical models that faithfully represent the system they are modelling.

This textbook introduces the intellectual framework for modelling with Comsol Multiphysics, a package which has unique features in representing multiply linked domains with complex geometry, highly coupled and nonlinear equation systems, and arbitrarily complicated boundary, auxiliary, and initial conditions. But with this modelling power comes great opportunities and great perils.

Progressively, in the first part of the book the novice modeler develops an understanding of how to build up complicated models piecemeal and test them modularly. The second part of the book introduces advanced analysis techniques. The final part of the book deals with case studies in a broad range of application areas including nonlinear pattern formation, thin film dynamics and heterogeneous catalysis, composite and effective media for heat, mass, conductivity, and dispersion, population balances, tomography, multiphase

About the author

William B. J. Zimmerman CEng FIChemE is the Professor of Biochemical Dynamical Systems in Chemical and Process Engineering at the University of Sheffield. His research interests are in fluid dynamics, reaction engineering, and microfluidic biotechnology. He is the author of Process Modelling and Simulation with Finite Element Methods (2004), the earlier version of this book, and the editor of Microfluidics: History, Theory and Applications (2005). He has previously created modules entitled Chemical Engineering Problem Solving with Mathematica, Modelling and Simulation in Chemical Processes, Numerical Analysis in Chemical Engineering, and FORTRAN programming. He has been modelling with finite element methods since 1986. He has authored over eighty scientific and scholarly works. He is a graduate of Princeton and Stanford Universities in Chemical Engineering, past Director of the MSc. in Environmental and Energy Engineering, originator of the MSc. in Process Fluid Dynamics, and a winner in US and UK national competitions of five prestigious fellowships.

*Stanislav Kasa*